*Int. J. Therm. Sci.* (2000) 39, 556–570

S1290-0729(00)00251-9/FLA

# Modelling of heat transport in beds packed with spherical particles for various bed geometries and/or thermal boundary conditions

Markus Winterberg, Evangelos Tsotsas *

*Laboratory for Thermal Process Engineering, Otto-von-Guericke-University Magdeburg, Universitätsplatz 2, D-39106 Magdeburg, Germany*

(Received 26 June 1999, accepted 17 December 1999)

**Abstract** — A quasi-homogeneous model for heat transport in packed beds with fluid flow (a so-called $\Lambda_r(r)$-model, explicitly accounting for laterally uneven distributions of porosity, flow velocity and effective thermal conductivity) is successfully compared with a comprehensive collection of experimental data from literature. Specifically, experiments with various bed geometries (slab, annular channel, circular tube) and several different boundary conditions at the wall (constant temperature, constant heat flux, adiabatic) are accurately described by the model without any adaption of its parameters. Furthermore, systematic comparison is conducted with an $\alpha_w$-model (plug-flow combined with a wall heat transfer coefficient). The comparison reveals advantages of the $\Lambda_r(r)$-model in predictive performance. These advantages, conceptual aspects, as well as better possibilities for considering temperature-dependent properties and simulating complex processes like reaction and adsorption justify the recommendation of the $\Lambda_r(r)$-model for practical use. © 2000 Éditions scientifiques et médicales Elsevier SAS

**packed beds / heat transport / modelling / flow maldistribution / thermal conductivity**

## Nomenclature

| | | |
|---|---|---|
| $c_f$ | specific heat capacity of the fluid | $J \cdot kg^{-1} \cdot K^{-1}$ |
| $B$ | width of a rectangular channel | m |
| $D$ | tube diameter | m |
| $d_p$ | particle diameter | m |
| $E$ | error index after equation (2) | |
| $F$ | error index after equation (6) | |
| $h_{ov}$ | overall heat transfer coefficient | $W \cdot m^{-2} \cdot K^{-1}$ |
| $K_1$ | slope parameter | |
| $K_2$ | damping parameter | |
| $L$ | length of the packed bed | m |
| $m$ | number of measured points per experiment | |
| $Nu_{ov}$ | overall Nusselt number $= h_{ov} d_p / \lambda_f$ | |
| $n$ | number of experiments per data group | |
| $Pe_0$ | molecular Péclet number $= \bar{u}_0 d_p \rho_f c_f / \lambda_f$ | |
| $Pr$ | Prandtl number | |
| $p$ | pressure | Pa |
| $R$ | tube radius | m |
| $Re_0$ | Reynolds number $= \rho_f \bar{u}_0 d_p / \eta_f$ | |
| $r$ | radial coordinate | m |
| $T$ | temperature | K or °C |
| $u_c$ | superficial velocity in the core of the bed | $m \cdot s^{-1}$ |
| $u_0$ | local superficial velocity | $m \cdot s^{-1}$ |
| $\bar{u}_0$ | average superficial velocity | $m \cdot s^{-1}$ |
| $x$ | lateral coordinate | m |
| $z$ | axial coordinate | m |

*Greek symbols*

| | | |
|---|---|---|
| $\alpha_w$ | wall heat transfer coefficient | $W \cdot m^{-2} \cdot K^{-1}$ |
| $\eta_{eff}$ | effective dynamic viscosity | Pa·s |
| $\eta_f$ | dynamic viscosity of the fluid | Pa·s |
| $\Lambda_{ax}$ | effective axial thermal conductivity | $W \cdot m^{-1} \cdot K^{-1}$ |
| $\Lambda_r$ | effective radial thermal conductivity | $W \cdot m^{-1} \cdot K^{-1}$ |
| $\Lambda_x$ | effective lateral thermal conductivity | $W \cdot m^{-1} \cdot K^{-1}$ |
| $\lambda_f$ | thermal conductivity of the fluid | $W \cdot m^{-1} \cdot K^{-1}$ |
| $\lambda_{bed}$ | effective thermal conductivity without fluid flow | $W \cdot m^{-1} \cdot K^{-1}$ |
| $\rho_f$ | density of the fluid | $kg \cdot m^{-3}$ |
| $\psi$ | local bed porosity | |
| $\psi_\infty$ | bed porosity of the infinitely extended bed | |
| $\bar{\psi}$ | average bed porosity | |

* Correspondence and reprints.
evangelos.tsotsas@vst.uni-magdeburg.de

*Subscripts*

| | |
|---|---|
| ax | axial |
| bed | of the bed, without fluid flow |
| c | core (at the core of the packed bed) |
| cyl | cylinder |
| eff | effective |
| exp | experimental |
| f | fluid |
| in | inlet |
| out | outlet |
| ov | overall |
| p | particle |
| r | radial |
| w | wall |
| $\infty$ | infinitely extended bed |

## 1. INTRODUCTION

Heat transport in packed beds with fluid flow is of considerable importance for processes like heterogeneous catalytic reaction, adsorption, chromatography, heat exchange or storage in chemical, pharmaceutical, environmental, energy and other industries. Temperature profiles are commonly calculated by a quasi-homogeneous model which assumes uniformity of porosity and fluid velocity over the cross section of the bed (plug flow), uses an effective, spatially constant lateral (for a tube: radial) thermal conductivity and introduces a heat transfer coefficient at the wall, $\alpha_w$. The latter is defined by means of a boundary condition of the third kind (temperature jump) at the wall of the bed. This standard model, which has been investigated or applied in hundreds of papers and is included in practically every text- or handbook, see, e.g., [1–3], will be called in the following the $\alpha_w$-model.

On the other hand, it has been recognized that the uniformity of bed structure is considerably disturbed by the rigid wall (Roblee et al. [4], among many others after them), giving rise to maldistribution of fluid flow (channeling, early observations by Schwartz and Smith [5]). It is reasonable to explicitly account for these effects in a—still quasi-homogeneous—model and to regard, by analogy, the effective lateral thermal conductivity as a function of the distance from the wall. A model of this kind is called, with reference to the case of a packed circular tube, a $\Lambda_r(r)$-model or wall heat conduction model. Though early versions of the $\Lambda_r(r)$-model were put forward by Smith and coworkers (e.g., [6]), enhanced development of the—computationally demanding—model took place in the eighties [7, 8], accompanied by considerable progress in better understanding and calculating packed beds reactors ([9, 10], among others).

On this basis, Winterberg et al. [11] have recently implemented an up-to-date version of the $\Lambda_r(r)$-model and derived all coefficients involved in the calculations of the profile of effective thermal conductivity by comparison with experimental data from literature. This reevaluation reveals several positive features of the wall heat conduction approach:

- Either constants—partly theoretically derivable—or very simple correlations are obtained for all model parameters involved in the calculation of the effective lateral thermal conductivity profile. Specifically, no dependence on the quotient between lateral bed dimension and particle diameter occurs. In this context, it is important to notice that such dependences are typical for the parameters of the $\alpha_w$-model (see, e.g., [12]).
- The real boundary condition is applied at the wall of the bed, avoiding, thus, the introduction of an artificial boundary condition of the third kind and of a wall heat transfer coefficient, $\alpha_w$, which is especially at small Reynolds numbers difficult to justify and correlate [13].
- The same model and the same set of coefficients can be successfully used without and with chemical reaction [14].

However, several restrictions are included in the work of Winterberg et al. [11] concerning the fluid (gas), the shape of the particles (spherical), the shape of the container of the bed (circular tube) and the thermal boundary condition at the wall (constant temperature). The last two restrictions define the major type of experiment that has been evaluated, namely heat transfer between the fluid entering at some prescribed temperature a packed, circular tube and the wall of this tube which is kept isothermal at some other temperature (Nusselt–Graetz experiment for a packed tube).

With the above-mentioned investigation as its starting point, the present paper follows a twofold objective:

- Find out, whether experimental results other than those used for its development can be accurately predicted by the $\Lambda_r(r)$-model of Winterberg et al. [11], or not. Specifically, data for bed geometries other than cylindrical and boundary conditions other than the constant wall temperature condition shall be analyzed. In this sense, the objective is to prove the invariability of model parameters upon changes of bed geometry and/or thermal boundary condition.
- Comprehensively compare the $\Lambda_r(r)$-model with the $\alpha_w$-model in terms of their predictive performances.

The restrictions to nearly spherical particles will remain, along with the restriction to gases (the latter with the exception for a few experimental runs with water). Though brief reference to chemical reactors will be given, data with chemical reactions will not be treated in the present paper.

## 2. DATA, MODELS AND METHODS

Primary classification of experimental data available from literature which will be evaluated in the present work is conducted in terms of bed geometry, distinguishing between slab, annular channel and circular tube (data groups D1, D2, D3, respectively). Further characterization is based on the thermal boundary condition at the wall or walls of the bed (constant temperature/BC of the first kind, constant heat flux/BC of the second kind, zero heat flux/adiabatic). In this way, a total of seven subgroups is defined as summarized in *table I*. One subgroup (D3.1, circular packed tube with constant wall temperature) has already been used by Winterberg et al. [11] in the development of the present $\Lambda_r(r)$-model and is included in the table for the sake of completeness. All other six subgroups have never before been confronted with this model and are, thus, significant for the intended check of its validity and predictability.

The three geometric configurations under investigation are depicted schematically in *figure 1*, along with pertinent coordinates and dimensions. Flow is always in the direction of the $z$-axis. Equations of the $\Lambda_r(r)$-model after Winterberg et al. [11] are summarized in the Appendix for every geometric configuration. Referring to the circular tube, remember that the radial porosity profile, $\psi(r)$, is calculated for nearly spherical particles after Giese [15], Giese et al. [16], equation (A.2). The respective velocity profile, $u_0(r)$, is obtained by numerical solution of the extended Brinkman equation (equation (A.3) with the effective viscosity, $\eta_{\mathrm{eff}}$, after the same authors, equation (A.4)). For the effective axial thermal conductivity the additive equation (A.6) is used, as proposed by many authors, e.g., Tsotsas [3]. Here, as well as in equation (A.8), the quiescent part, i.e. the effective thermal conductivity of the packed bed without fluid flow, $\lambda_{\mathrm{bed}}$, is calculated after Zehner and Schlünder [17] as a function of the local porosity. Of distinctive importance for the model is the part of the effective radial thermal conductivity $\Lambda_r(r)$, which depends on fluid flow, i.e. the second right-hand term of equation (A.8). This is proportional to the superficial fluid velocity in the core of the bed (at $r = 0$), $u_c$, compare also with [18]. Proportionality is specified by the so-called slope parameter, $K_1$, a constant after equation (A.10). Finally, the damping parameter $K_2$ (equations (A.9), (A.11)) determines in multiples of the particle diameter $d_p$ the point, beyond which $\Lambda_r(r)$ begins to decline towards the wall. Notice that the argument of the exponential function, which was $(-Re_0/70)$ in [11], has been replaced by $(-Pe_0/50)$ in equation (A.11). Both expressions are identical for $Pr = 0.71$ (ambient air as the fluid). The modification has to do with the use of some data with water in the present work, and is of no significance for the evaluation of data with gases by Winterberg et al. [11]. This aspect will be further discussed in connection with data group D1. After equation (A.11) the zone of inhibited heat transport is reduced to a small region of $0.44\, d_p$ near the wall for high Péclet numbers, at low Péclet numbers it expands considerably. However, in the region of low Péclet numbers both the convective part of the effective thermal conductivity $\Lambda_r(r)$ and the model sensitivity upon $K_2$ are relatively low. More details on the $\Lambda_r(r)$-model can be obtained from the original work of Winterberg et al. [11], including exemplary velocity and thermal conductivity profiles, aspects of physical interpretation and additional background literature.

Transcription to Cartesian coordinates of the slab is straightforward. In this case, the porosity, velocity and thermal conductivity functions are symmetrical in respect to the plane with $x = B/2$. Notice that the dependence of the physical properties entering the extended Brinkman equation on temperature is ignored, enabling its separate solution. The general term of a $\Lambda_r(r)$-model is used in spite of the replacement of the radial coordinate $r$ by $x$. For the annular duct, porosity and effective radial thermal conductivity (equations (A.12), (A.13)) are treated symmetrically to $r = (R + r_{\mathrm{cyl}})/2$, i.e. the influence of different curvatures of the two cylindrical walls is neglected (see also *figure 1*). The core superficial velocity, $u_c$, is also calculated at $r = (R + r_{\mathrm{cyl}})/2$. For every geometry, numerical solutions of the energy balances (equation (A.1), (A.14), respectively) requires the specification of the thermal boundary conditions at the inlet, at the outlet and at the wall. Boundary conditions used in the present work are recapitulated in *table II*, additional explanations on individual subgroups (compare with *table I*) will be given in the course of the presentation of the respective results.

A great number of different versions of the $\alpha_w$-model exist in literature. The present authors regard the model version of Martin and Nilles [19] to be the most efficient, because of the large number and wide range of underlying experimental results (the main part of data of subgroup D3.2, *table I*), its documented satisfactory

TABLE I
Summary of the experiments reevaluated in the present work. NE: number of reevaluated experiments, NP: number of measured points.

| | Geometry | Experimental boundary conditions | Authors | Experimental parameters | Numbers of experiments | Error |
|---|---|---|---|---|---|---|
| D1 | slab | $T_{w,1} = \text{const}$<br>$T_{w,2} = \text{const}$ | Schröder et al. [21]<br>Bey and Eigenberger [22] | F: air, water<br>P: glass<br>$d_p = 2.0$–$10.0$ mm<br>$B/d_p = 6.1$–$26.0$<br>$Re_0 = 97$–$481$ | NE: 8<br>NP: 108 | $\overline{E}(\Lambda_r(r)) = 3.35\,\%$<br>$\overline{E}(\alpha_w) = 3.28\,\%$ |
| D2.1 | annular channel | $T_{cyl} = \text{const}$<br>$T_w = \text{const}$ | Yagi and Kunii [23]<br>Baddour and Yoon [24] | F: air<br>P: glass, ceramic<br>$d_p = 0.9$–$7.9$ mm<br>$(D - d_{cyl})/d_p = 16.0$–$51.1$<br>$Re_0 = 32$–$705$ | NE: 3<br>NP: 33 | $\overline{E}(\Lambda_r(r)) = 3.06\,\%$<br>$\overline{E}(\alpha_w) = 3.46\,\%$ |
| D2.2 | annular channel | $T_{cyl} = \text{const}$<br>$\dot{q}_w = 0$ | Gabor [25]<br>Botterill and Denloye [26] | F: air<br>P: sand, copper, synthetics<br>$d_p = 0.6$–$3.2$ mm<br>$(D - d_{cyl})/d_p = 22.8$–$101.3$<br>$Re_0 = 11$–$540$ | NE: 95<br>NP: – | $\overline{F}(\Lambda_r(r)) = 25.27\,\%$<br>$\overline{F}(\alpha_w) = 27.95\,\%$ |
| D2.3 | annular channel | $\dot{q}_{cyl} = \text{const}$<br>$\dot{q}_w = 0$ | Sordon [27] | F: argon<br>P: ceramic<br>$d_p = 4.0$ mm<br>$(D - d_{cyl})/d_p = 21.5$<br>$Re_0 = 85$ | NE: 2<br>NP: 72 | $\overline{E}(\Lambda_r(r)) = 2.53\,\%$<br>$\overline{E}(\alpha_w) = 3.07\,\%$ |
| D2.4 | annular channel | $\dot{q}_{cyl} = \text{const}$<br>$T_w = \text{const}$ | Sordon [27] | F: argon<br>P: ceramic<br>$d_p = 4.0$ mm<br>$(D - d_{cyl})/d_p = 21.5$<br>$Re_0 = 67$–$155$ | NE: 4<br>NP: 144 | $\overline{E}(\Lambda_r(r)) = 2.41\,\%$<br>$\overline{E}(\alpha_w) = 4.27\,\%$ |
| D3.1 | circular tube | $T_w = \text{const}$ | see [11] | F: air, $N_2$, $NH_3$<br>P: glass, ceramic, synthetics<br>$d_p = 2.0$–$12.7$ mm<br>$D/d_p = 4.9$–$33.3$<br>$Re_0 = 18$–$1\,818$ | NE: 49<br>NP: 447 | $\overline{E}(\Lambda_r(r)) = 4.75\,\%$<br>$\overline{E}(\alpha_w) = 6.61\,\%$ |
| D3.2 | circular tube | $\dot{q}_w = \text{const}$ | Seidel [29]<br>Quinton and Storrow [28]<br>Martin and Nilles [19] | F: air<br>P: glass, ceramic<br>$d_p = 1.1$–$20.0$ mm<br>$D/d_p = 4.7$–$51.0$<br>$Re_0 = 1.5$–$1\,396$ | NE: 66<br>NP: 1 241 | $\overline{E}(\Lambda_r(r)) = 8.24\,\%$<br>$\overline{E}(\alpha_w) = 9.38\,\%$ |

accuracy and actual recommendations for practical application [3]. Therefore, this version will be used for comparison with the $\Lambda_r(r)$-model. Following Martin and Nilles [19], their own correlation is applied for the wall heat transfer coefficient $\alpha_w$ (see *table II* for the respective boundary conditions of the third kind), while the, now spatially constant, effective lateral thermal conductivity $\Lambda_r$ is calculated after Bauer and Schlünder [20]. Axial dispersion of heat is accounted for by analogy to equation (A.6), quiescent thermal conductivity is calculated

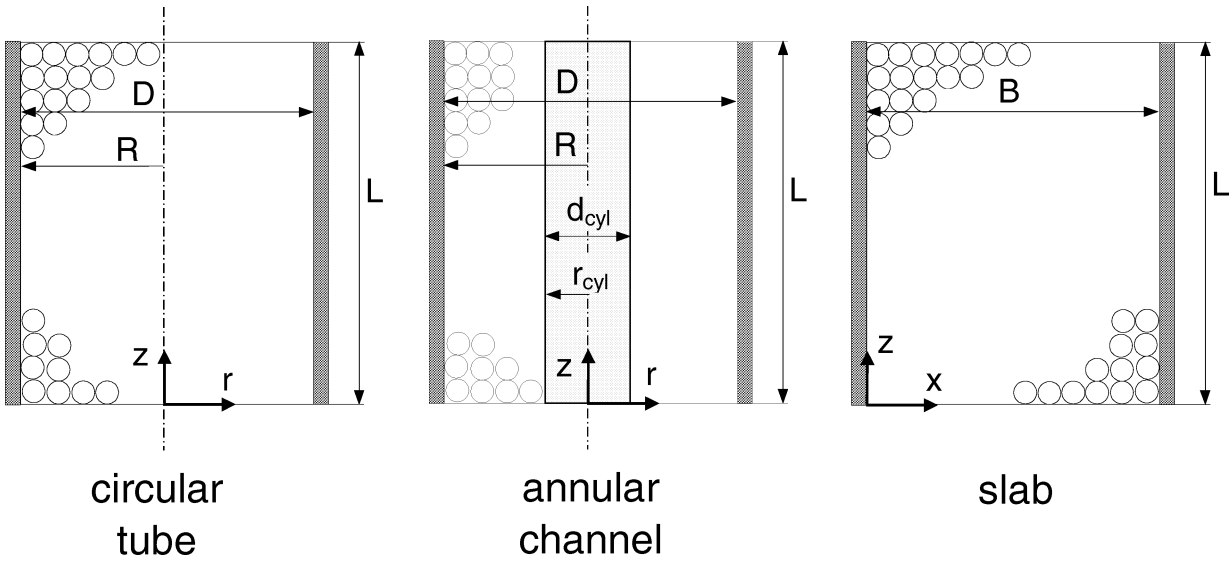


**Figure 1.** Geometric configurations analyzed in the present work with respective dimensions and coordinates.

after Zehner and Schlünder [17]. Further equations are not necessary, because both bed porosity and flow velocity are set to constant values in the $\alpha_w$-model (plug flow assumption with $\bar{\psi}$ and $\bar{u}_0$).

More difficult is the definition of a quantitative index for the discrepancy between observed and calculated profiles, and for the comparison of predictive performance of the two models. Winterberg et al. [11] proposed to this purpose

$$\chi^2 = \frac{1}{m}\sum_{i=1}^{m}\left(\frac{T_{\mathrm{exp},i} - T_i}{T_{\mathrm{exp},i}}\right)^2 \qquad (1)$$

i.e. the sum of squared differences between calculated, $T_i$, and measured, $T_{\mathrm{exp},i}$, temperatures, related to the latter and to the number of measured points of one temperature profile, $m$. However, this definition has the disadvantage of dependence on the average level of absolute temperature, and is implicit in respect of approximate average deviation in centigrades. For this reason, another index is used in the present work, namely the average error

$$E = \frac{1}{m}\sum_{i=1}^{m}\left|\frac{T_{\mathrm{exp},i} - T_i}{\Delta T}\right| \qquad (2)$$

Linear definition and the introduction of $\Delta T$ as a temperature difference characteristic of the experiment under consideration, typically a maximal temperature difference, are a choice for simplicity of interpretation. For instance, $\Delta T$ is the difference between wall and fluid inlet temperature in an experiment of subgroup D3.1. With $\Delta T = 100$ K, $E = 0.02$ implies an average temperature difference between calculation and experiment of 2 K. Individual definitions of $\Delta T$ will be given for every subgroup of data, with the exception of subgroup D2.2, whose different treatment will be explained later on. Since $E$ after equation (2) refers to one certain temperature profile, the average

$$\overline{E} = \frac{1}{n}\sum_{i=1}^{n} E_i \qquad (3)$$

is used in order to express the overall performance for one experimental subgroup. Here, $n$ is the total number of runs in the subgroup, identical to the number of reevaluated experiments, NE, after *table I*.

It should be borne in mind that limits are set to the comparability between different subgroups (*table I*), or even between different experiments in one and the same subgroup, on the basis of an error index like $E$ or $\overline{E}$. Furthermore, apart from equations (2) and (3) many other definitions of an error index are possible (e.g., definitions weighing by local resolution or flow velocity), each with specific advantages. Preliminary investigations have shown that it is possible to moderately shift values of the error index for different subgroups and/or models relatively to each other by changing its definition. However, such variations are not significant at the level of overall comparison between the $\Lambda_r(r)$- and the $\alpha_w$-model.

TABLE II
Summary of the boundary conditions (BC) used to solve the model equations of the $\Lambda_r(r)$- and the $\alpha_w$-model.

| | BC at the inlet/outlet | BC at the walls, $\Lambda_r(r)$-model | BC at the walls, $\alpha_w$-model |
|---|---|---|---|
| D1 | $z=0$: $T=\overline{T}_{in}$<br>$z=L$: $\frac{\partial T}{\partial z}=0$ | $x=0$: $T=T_{w,1}$<br>$x=B$: $T=T_{w,2}$ | $x=0$: $\Lambda_x \frac{\partial T}{\partial x}=\alpha_w(T-T_{w,1})$<br>$x=B$: $-\Lambda_x \frac{\partial T}{\partial x}=\alpha_w(T-T_{w,2})$ |
| D2.1 | $z=0$: $T=\overline{T}_{in}$ or $T=T_{in}(r)$<br>$z=L$: $\frac{\partial T}{\partial z}=0$ | $r=r_{cyl}$: $T=T_{cyl}$<br>$r=R$: $T=T_w$ | $r=r_{cyl}$: $\Lambda_r \frac{\partial T}{\partial r}=\alpha_w(T-T_{cyl})$<br>$r=R$: $-\Lambda_r \frac{\partial T}{\partial r}=\alpha_w(T-T_w)$ |
| D2.2 | $z=0$: $T=\overline{T}_{in}$<br>$z=L$: $\frac{\partial T}{\partial z}=0$ | $r=r_{cyl}$: $T=T_{cyl}$<br>$r=R$: $\frac{\partial T}{\partial r}=0$ | $r=r_{cyl}$: $\Lambda_r \frac{\partial T}{\partial r}=\alpha_w(T-T_{cyl})$<br>$r=R$: $\frac{\partial T}{\partial r}=0$ |
| D2.3 | $z=0$: $T=\overline{T}_{in}$<br>$z=L$: $\frac{\partial T}{\partial z}=0$ | $r=r_{cyl}$: $T=T_{cyl}(z)$<br>$r=R$: $\frac{\partial T}{\partial r}=0$ | $r=r_{cyl}$: $\Lambda_r \frac{\partial T}{\partial r}=\alpha_w(T-T_{cyl}(z))$<br>$r=R$: $\frac{\partial T}{\partial r}=0$ |
| D2.4 | $z=0$: $T=\overline{T}_{in}$<br>$z=L$: $\frac{\partial T}{\partial z}=0$ | $r=r_{cyl}$: $T=T_{cyl}(z)$<br>$r=R$: $T=T_w$ | $r=r_{cyl}$: $\Lambda_r \frac{\partial T}{\partial r}=\alpha_w(T-T_{cyl}(z))$<br>$r=R$: $-\Lambda_r \frac{\partial T}{\partial r}=\alpha_w(T-T_w)$ |
| D3.1 | $z=0$: $T=\overline{T}_{in}$ or $T=T_{in}(r)$<br>$z=L$: $\frac{\partial T}{\partial z}=0$ | $r=0$: $\frac{\partial T}{\partial r}=0$<br>$r=R$: $T=T_w$ | $r=0$: $\frac{\partial T}{\partial r}=0$<br>$r=R$: $-\Lambda_r \frac{\partial T}{\partial r}=\alpha_w(T-T_w)$ |
| D3.2 | $z=0$: $T=\overline{T}_{in}$ or $T=T_{in}(r)$<br>$z=L$: $\frac{\partial T}{\partial z}=0$ | $r=0$: $\frac{\partial T}{\partial r}=0$<br>$r=R$: $T=T_w(z)$ | $r=0$: $\frac{\partial T}{\partial r}=0$<br>$r=R$: $-\Lambda_r \frac{\partial T}{\partial r}=\alpha_w(T-T_w(z))$ |

## 3. EVALUATION FOR THE SLAB: DATA GROUP D1

The first type of reexamined measurements are experiments of heat transfer between two parallel plates, heated or cooled at constant temperatures, $T_{w,1}$ and $T_{w,2}$, respectively. The gap is packed with particles, flow is parallel to the plates. The side walls of the arrangement are insulated, so that the two-dimensional geometry of an infinite slab (*figure 1*, group D1 in *table I*) may be assumed. The test section is sufficiently long for transforming any inlet fluid temperature distribution into a fully developed lateral temperature profile, which does not depend any more on the axial coordinate and is measured at $z = L$ within or immediately after the packing. Experiments of this kind have been performed by Schröder et al. [21] and by Bey and Eigenberger [22]. Schröder et al. worked with water, Bey and Eigenberger used air as the fluid. All packings consisted of monodispersed glass spheres. The dimensionless width $B/d_p$ ranged between 6.1 and 26.0, the Reynolds number $Re_0$ varied from 97 to 481.

While in the $\Lambda_r(r)$-model the real boundary condition of the first kind ($T_w = \text{const}$) is used at the heated or cooled plate, artificial wall boundary conditions of the third kind are formulated for the $\alpha_w$-model, see *table II*. In both works reevaluated here, the authors operate with

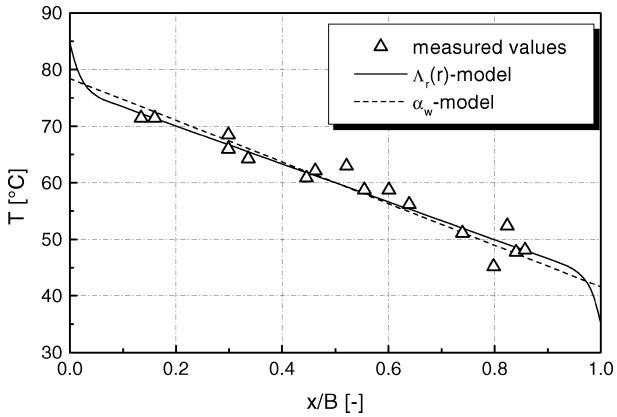


**Figure 2.** Measured and calculated temperature profiles in a packed slab (data group D1). Experimental data after Bey and Eigenberger [22], fluid: air, solid: glass, $B/d_\mathrm{p} = 6.1$, $Re_0 = 481$; $E(\Lambda(r)) = 3.24\,\%$, $E(\alpha_\mathrm{w}) = 3.61\,\%$.

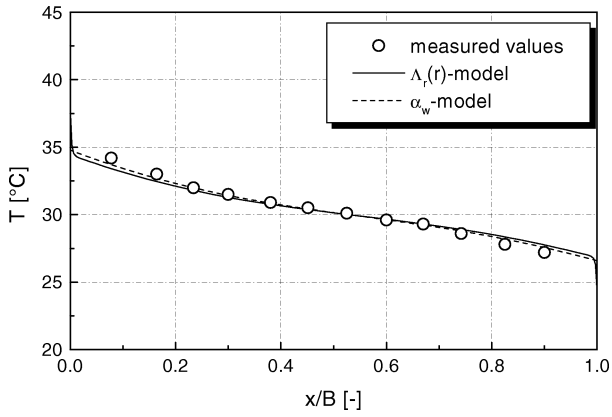


**Figure 3.** Measured and calculated temperature profiles in a packed slab (data group D1). Experimental data after Schröder et al. [21], fluid: water, solid: glass, $B/d_\mathrm{p} = 26.0$, $Re_0 = 405$; $E(\Lambda(r)) = 1.90\,\%$, $E(\alpha_\mathrm{w}) = 1.21\,\%$.

constant inlet temperature, so that the boundary condition at $z = 0$ is set by respective values from the original papers. Consequently, the complete evolution of temperature field between inlet and the level of measurement is calculated by the models. According to the usual practice (see, e.g., [3]) flat profiles are assumed at the outlet for this as well as for all other reevaluated experiments (*table II*). The temperature difference involved in the definition of the error index $E$ (equation (2)) is set equal to $\Delta T = T_{\mathrm{w},1} - T_{\mathrm{w},2}$, i.e. to the temperature difference between the plates.

In *figure 2* results of computations with the two different models for an experiment of Bey and Eigenberger [22] are depicted exemplarily. It can be seen that the deviation between the two different model predictions is relatively small in the core of the packed bed, where most measured points lie. Similar values of the effective lateral thermal conductivity $\Lambda_x$ are the reason for this behaviour. While $\Lambda_x/\lambda_\mathrm{f} = 41.1$ after Bauer and Schlünder [20] is used in the $\alpha_\mathrm{w}$-model over the whole channel cross section, the $\Lambda_r(r)$-model predicts a value $\Lambda_x/\lambda_\mathrm{f} = 45.5$ in the centre of the slab. The impact of different boundary conditions is obvious at the channel walls. The $\Lambda_r(r)$-model operates with the real wall temperatures, here $T_{\mathrm{w},1} = 85\,^\circ\mathrm{C}$ and $T_{\mathrm{w},2} = 35\,^\circ\mathrm{C}$, respectively, while the $\alpha_\mathrm{w}$-model predicts temperature jumps. However, the overall influence of the boundary condition is not very large, leading to similar error indices, $E(\alpha_\mathrm{w}) = 3.61\,\%$ and $E(\Lambda_r(r)) = 3.24\,\%$. An orientation mark for this predictive performance can be derived from the linear profile connecting the above mentioned wall temperatures. This profile would be valid in the absence of any maldistribution or wall resistance irrespectively of the value of the effective lateral thermal conductivity, though heat flux between the plates would be proportional to the latter. For this limiting case a significantly, but not dramatically, higher error index of $E = 7.47\,\%$ is obtained.

A similar behaviour at even better accuracy ($E(\alpha_\mathrm{w}) = 1.21\,\%$ and $E(\Lambda_r(r)) = 1.90\,\%$) is obtained for the temperature profile from [21] that is presented in *figure 3*. Here, thermally fully developed conditions have been approximated but not completely reached, as the slight curvature of experimental and calculated profiles in the middle of the bed indicates. The data of Schröder et al. [21] are the only ones with a liquid (water) in the present investigation. Their reasonable and more accurate treatment by the $\Lambda_r(r)$-model led to the slight modification of the damping parameter $K_2$ which has been described in the previous section. As already pointed out, this modification is of no significance for the simulation of data with gases under usual test conditions. Certainly, more data with liquids are necessary for a comprehensive and final recommendation.

Similar results are found when the computations are extended to other experiments of the data group D1. In *figure 4* the error indices $E(\Lambda_r(r))$ of predictions by the $\Lambda_r(r)$-model are plotted over the error indices $E(\alpha_\mathrm{w})$ of the $\alpha_\mathrm{w}$-approach. If the two models described the measured values with the same accuracy, all points would lie on a straight line with the slope of one. This does not happen for every individual point, but is approximately true on the average, as the indices $\overline{E}(\Lambda_r(r)) = 3.35\,\%$ and $\overline{E}(\alpha_\mathrm{w}) = 3.28\,\%$ after equation (3) show (*table I*). In spite of the value of data group D1, it is rather risky to base packed bed modelling only on it. This can be

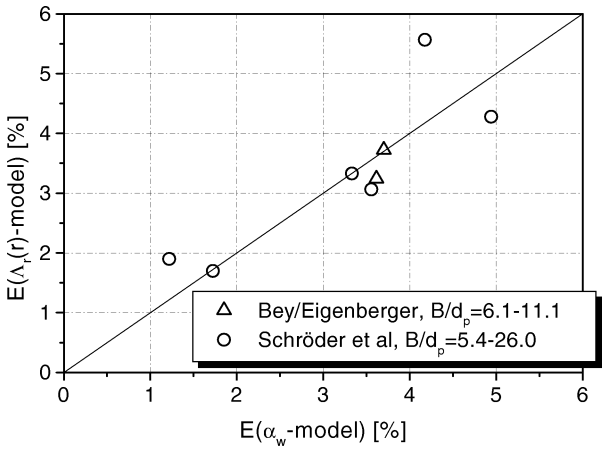


**Figure 4.** Comparison between the $\Lambda_r(r)$-model after Winterberg et al. [11] and the $\alpha_w$-model of Martin and Nilles [19] with respect to the predictive performance for the slab geometry (data group D1).

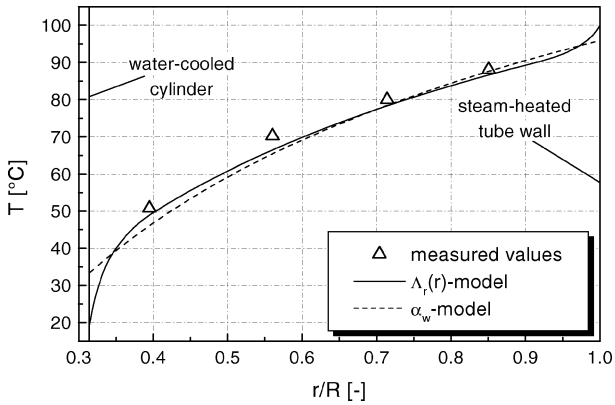


**Figure 5.** Measured and calculated temperature profiles in an annular channel (data subgroup D2.1). Experimental data after Yagi and Kunii [23], fluid: air, solid: glass, $(D-d_{cyl})/d_p = 17.5$, $Re_0 = 131$; $E(\Lambda(r)) = 2.85\,\%$, $E(\alpha_w) = 3.73\,\%$.

underlined by comparison of early efforts towards an $\Lambda_r(r)$-model (e.g., [7], referring only to the experiments by Schröder et al. [21]) with [11] as well as with the present work.

## 4. EVALUATION FOR THE ANNULAR CHANNEL: DATA GROUP D2

Data group D2 refers to the annular channel geometry (*figure 1*), realized by placing a heating or cooling cylinder in the centre of a circular tube and filling the gap with particles. By heating or cooling with fluid media, electrical heating or insulation various combinations of wall boundary conditions are possible and make distinction between four subgroups necessary (*table I*). Wall boundary conditions entering calculation with the $\Lambda_r(r)$- or the $\alpha_w$-model are recapitulated in *table II*, along with inlet and outlet boundary conditions.

Subgroup D2.1 is very similar to data group D1, because the walls of the channel are kept isothermal at different temperatures. The respective difference, $\Delta T = T_w - T_{cyl}$, is, again, used as the characteristic difference in the definition of the error index after equation (2). Experiments have been reported by Yagi and Kunii [23] and by Baddour and Yoon [24]. In order to obtain thermally fully developed conditions, Yagi and Kunii controlled—and measured—the inlet temperature profile to the vicinity of what they have expected at the outlet. Baddour and Yoon used isothermal inflow (*table II*) and a column sufficiently long for suppressing the influence of inlet conditions. Packings consisted of glass or ceramic spheres. The ratio between the total width of the annular channel and the particle diameter $(D-d_{cyl})/d_p$ ranged between 16.0 and 51.1, the Reynolds number between 32 and 705 (see *table I*). *Figure 5* shows exemplarily one measured temperature profile from [23]. The inner cylinder is cooled with water, the outer tube wall is heated with steam. Prediction by the $\alpha_w$-model is good, prediction by the $\Lambda_r(r)$-model is better ($E(\Lambda_r(r)) = 2.85\,\%$, $E(\alpha_w) = 3.73\,\%$). That is also true for the other experiments of subgroup D2.1, leading to moderate advantages of the $\Lambda_r(r)$-model in terms of the average error index $\overline{E}$ (see *table I*).

Experimental data of Gabor [25] and Botterill and Denloye [26] from an annular channel with constant temperature at the inner and insulation of the outer cylinder constitute subgroup D2.2 (*tables I, II*). The inner cylinder was an immersed electrical heater, as typically used in experiments with fluidized beds, with its surface temperature kept constant by control and uniform by the high thermal conductivity of its material. From this temperature, and from the measured mean inlet and outlet temperatures, the authors calculate overall heat transfer coefficients, $h_{ov}$, and overall Nusselt numbers, $Nu_{ov}$, and report them without the underlying temperature values. Packings of sand, copper and synthetics have been used. The ratio $(D-d_{cyl})/d_p$ varied from 22.8 to 101.3, the Reynolds number from 11 to 540.

In reevaluation, the radial outlet temperature profile, $T_{out}(r)$, is calculated, and the mean outlet temperature $\overline{T}_{out}$ is derived by accounting for cylindrical geometry in the $\alpha_w$-model. For the $\Lambda_r(r)$-model, $\overline{T}_{out}$ is a caloric average (mixing cup temperature). Then, the overall heat transfer coefficient and the respective Nusselt number are

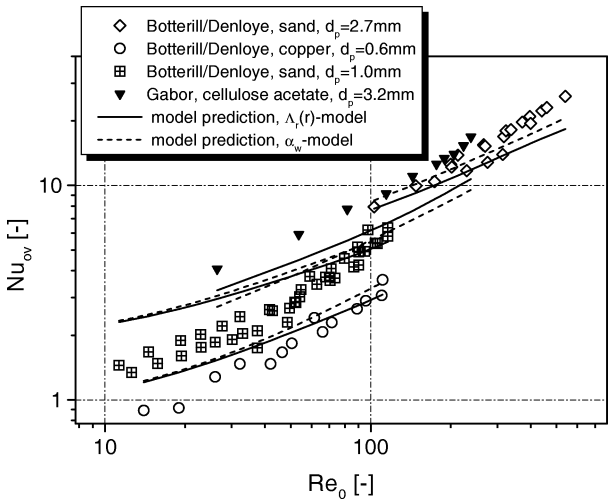


**Figure 6.** Measured and calculated overall Nusselt numbers from experiments in an annular channel (data subgroup D2.2). Experimental data after Gabor [25] and Botterill and Denloye [26], fluid: air, $(D-d_{\mathrm{cyl}})/d_{\mathrm{p}} = 22.8$–$51.1$, $Re_0 = 32$–$540$.

obtained by the same formulae as in the original papers, namely

$$h_{\mathrm{ov}} = \frac{\rho_{\mathrm{f}} c_{\mathrm{f}} \bar{u}_0 (R^2 - r_{\mathrm{cyl}}^2)}{2 r_{\mathrm{cyl}} L} \ln \frac{T_{\mathrm{w}} - \overline{T}_{\mathrm{in}}}{T_{\mathrm{w}} - \overline{T}_{\mathrm{out}}} \tag{4}$$

$$Nu_{\mathrm{ov}} = \frac{h_{\mathrm{ov}} d_{\mathrm{p}}}{\lambda_{\mathrm{f}}} \tag{5}$$

Comparison is conducted at the level of overall Nusselt numbers in *figure 6*. To cope with this, we deviate from equations (2), (3) and define the mean error as

$$\overline{F} = \frac{1}{n} \sum_{i=1}^{n} \left| \frac{Nu_{\mathrm{ov,exp},i} - Nu_{\mathrm{ov,calc},i}}{Nu_{\mathrm{ov,exp},i}} \right| \tag{6}$$

leading to values of of $\overline{F} = 25.27\,\%$ for the $\Lambda_r(r)$- and $\overline{F} = 27.95\,\%$ for the $\alpha_{\mathrm{w}}$-model (*table I*). These numbers are relatively large, mainly because of the definition (see previous discussion about restrictions in direct comparability of different error indices). Additional aspects are difficulties with the accurate determination of mean outlet temperature and the use of rather irregularly shaped and polydispersed particles by the original investigators. In spite of all this, agreement between calculation and measurement is satisfactory, with slight advantages of the $\Lambda_r(r)$-model.

The next sets of experiments reevaluated for the annular channel have been reported by Sordon [27]. He placed an electrically heated cylinder in the centre of a packed tube and operated with two different boundary

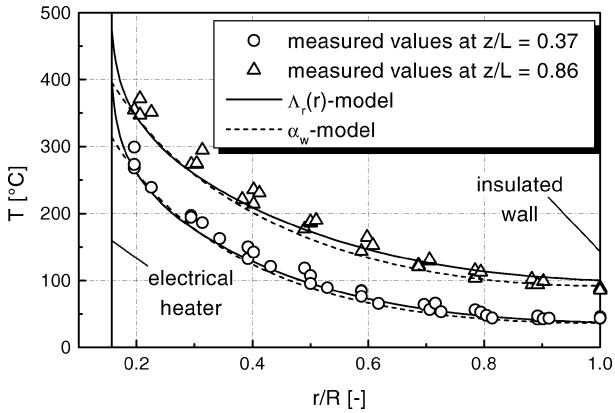


**Figure 7.** Measured and calculated temperature profiles in an annular channel (data subgroup D2.3). Experimental data after Sordon [27], fluid: argon, solid: alumina, $(D-d_{\mathrm{cyl}})/d_{\mathrm{p}} = 21.5$, $Re_0 = 85.2$; $z/L = 0.37$: $E(\Lambda(r)) = 2.15\,\%$, $E(\alpha_{\mathrm{w}}) = 2.78\,\%$, $z/L = 0.86$: $E(\Lambda(r)) = 2.90\,\%$, $E(\alpha_{\mathrm{w}}) = 3.36\,\%$.

conditions at the outer tube wall. On the one hand, he insulated the tube wall, realizing the boundary condition of zero heat flux at the wall (subgroup D2.3). On the other hand, he cooled the tube with water at constant temperature (subgroup D2.4, see *table I*). In contrast to the experiments of subgroup D2.2, no uniform cylinder temperature has been realized by Sordon. However, the respective axial temperature profile, $T_{\mathrm{cyl}}(z)$, has been measured and reported, and is used in the boundary condition at $r = r_{\mathrm{cyl}}$ (*table II*) (operating with values of heat flux would require modelling of the heating element and be indirect and less accurate). Sordon used argon as the fluid and ceramic packing material. The ratio of total width of channel cross section to particle diameter was constant at $(D-d_{\mathrm{cyl}})/d_{\mathrm{p}} = 21.5$, Reynolds number varied between 67 and 155.

Measured temperature profiles at two different bed lengths are shown in *figure 7* for an experiment with insulated tube wall (subgroup D2.3). The profiles indicate thermally fargoing developed conditions. The predictive performance of the $\Lambda_r(r)$-model is, again, excellent. Similar results are delivered by the $\alpha_{\mathrm{w}}$-model at the insulated wall (here the boundary condition is the same, see *table II*). At the heated wall, the temperature jump predicted by the $\alpha_{\mathrm{w}}$-model amounts to over 80 K, creating potentially significant deviations from the $\Lambda_r(r)$-approach. In the definition of error indices for the data of Sordon after equation (2) the maximal temperature difference between heated wall and bed at one and the same axial level has been used as $\Delta T$. Respective results are listed in *table I*.

Error indices of the $\Lambda_r(r)$-model are compared with respective values of the $\alpha_{\mathrm{w}}$-model for the entire data

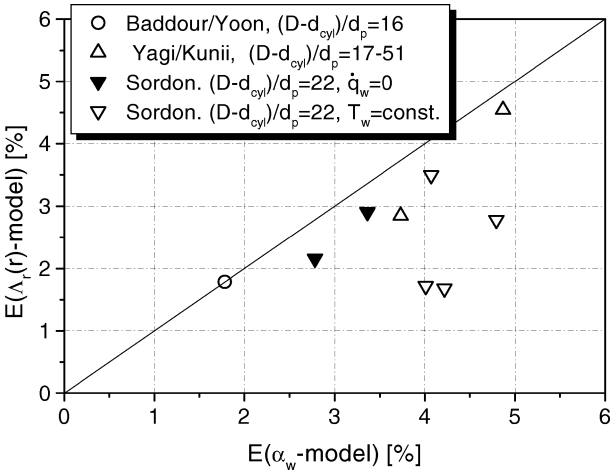


**Figure 8.** Comparison between the $\Lambda_r(r)$-model after Winterberg et al. [11] and the $\alpha_w$-model of Martin and Nilles [19] with respect to the predictive performance for experiments in annular channels (data group D2).

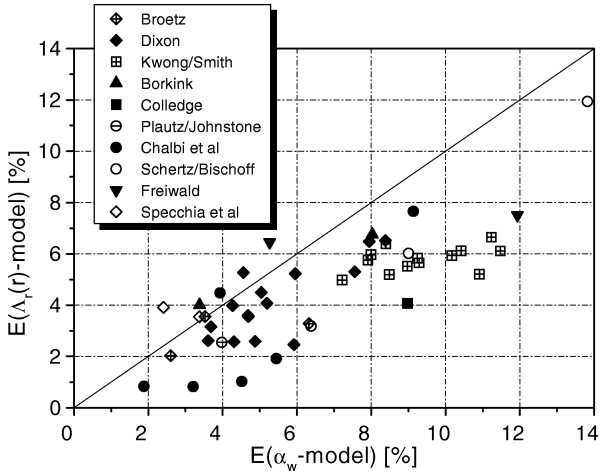


**Figure 9.** Comparison between the $\Lambda_r(r)$-model after Winterberg et al. [11] and the $\alpha_w$-model of Martin and Nilles [19] with respect to the predictive performance for experiments in packed circular tubes with constant wall temperature (data subgroup D3.1); for references see Winterberg et al. [11].

group D2 with the exception of subgroup D2.2 in *figure 8*, which is analogous to *figure 4*. Significant advantages of the wall heat conduction approach are observed at an, in general, very satisfactory level of predictive accuracy.

## 5. EVALUATION FOR THE CIRCULAR TUBE: DATA GROUP D3

The third group of reevaluated data refers to the classical and elementarily important geometry of the circular tube. Subgroup D3.1 contains the same data from experiments with packed tubes cooled or heated at constant wall temperature which have been used by Winterberg et al. [11] for the development of the present $\Lambda_r(r)$-model. With reference to *table I*, *table II* and to the original work, we will restrict the present discussion to the evaluation of the error index $E$ after equation (2), with $\Delta T$ equal to the temperature difference between wall and inlet fluid, which is new. Respective results for the $\Lambda_r(r)$- and for the $\alpha_w$-model are recapitulated in *figure 9*, averages are given in *table I*. *Figure 9* can be directly compared with figure 11 of the original paper [11], where the same evaluation has been conducted in terms of the $\chi^2$-factor (equation (1)). The comparison reveals that numerical values depend, as already pointed out, on the specific definition of the error index and that a certain shift of individual points can appear. However, the general trend remains the same, indicating the significance of better overall predictive performance of the $\Lambda_r(r)$-model according to both figures, see *figure 9*.

Changing the boundary condition at the wall of the circular tube from constant temperature to constant heat flux, subgroup D3.2 is obtained. This large subgroup contains the data of Quinton and Storrow [28], Seidel [29], and Martin and Nilles [19], *table I*. All authors used air as the fluid. The packings consisted of monodispersed spherical particles of low thermal conductivity. The diameter ratio $D/d_p$ ranged between 4.7 and 51.0, the Reynolds number between 1.5 and 1 396. Quinton and Storrow as well as Martin and Nilles heated the wall electrically, while Seidel used cooling air and approximated the boundary condition of the second kind ($\dot{q}_w = \text{const}$) by keeping the temperature difference between wall and the bulk of the bed as constant as possible. All authors measured and reported the wall temperature profile $T_w(z)$. As already practiced for subgroups D2.3, D2.4, these experimental profiles are inserted into the boundary conditions at $r = R$ for model resolution, see *table II*. Quinton and Storrow measured only the mean inlet temperature, therefore the boundary condition $T = \overline{T}_{in} = \text{const}$ is used at $z = 0$ for the reevaluation. The other authors report measured radial inlet temperature profiles. Such a radial profile is approximated with a fit function, which builds the boundary condition at the inlet ($T = T_{in}(r)$, *table II*). The reference temperature difference $\Delta T$ in equation (2) is equal to the maximal temperature difference between wall and core of the bed ($r = 0$) at $z = \text{const}$ (compare, again, with subgroups D2.3, D2.4).

It is important to notice that the $\alpha_w$-model which is used in the present work has been developed on the ba-

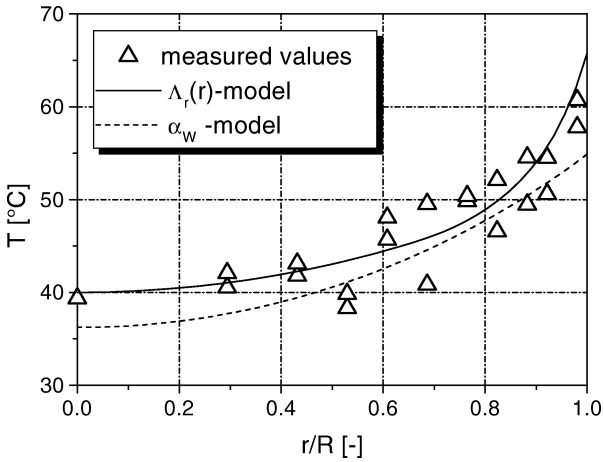


**Figure 10.** Measured and calculated temperature profiles in a packed circular tube with constant heat flux at the wall (data subgroup D3.2). Experimental data after Nilles and Martin [19], fluid: air, solid: ceramic, $D/d_\mathrm{p} = 5.1$, $Re_0 = 159$; $E(\Lambda(r)) = 9.51\,\%$, $E(\alpha_\mathrm{w}) = 12.72\,\%$.

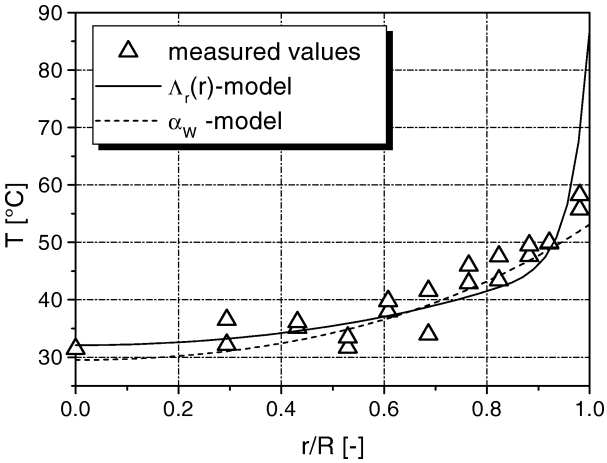


**Figure 11.** Measured and calculated temperature profiles in a packed circular tube with constant heat flux at the wall (data subgroup D3.2). Experimental data after Nilles and Martin [19], fluid: air, solid: ceramic, $D/d_\mathrm{p} = 5.1$, $Re_0 = 1\,128$; $E(\Lambda(r)) = 6.15\,\%$, $E(\alpha_\mathrm{w}) = 4.75\,\%$.

sis of the experiments of Martin and Nilles [19], which, on their turn, build the overwhelming majority in the subgroup D3.2. Consequently, the agreement between subgroup D3.2 data and the $\alpha_\mathrm{w}$-model is expected to be good, while the subgroup constitutes a real test for the $\Lambda_r(r)$-model. Examples of success in absolving this test are presented in *figures 10* and *11*, which are based on experimental data of Martin and Nilles [19] for two different Reynolds numbers. The $\Lambda_r(r)$-model predicts the data with similar accuracy as the $\alpha_\mathrm{w}$-model, while the deviation between the two approaches is maximal

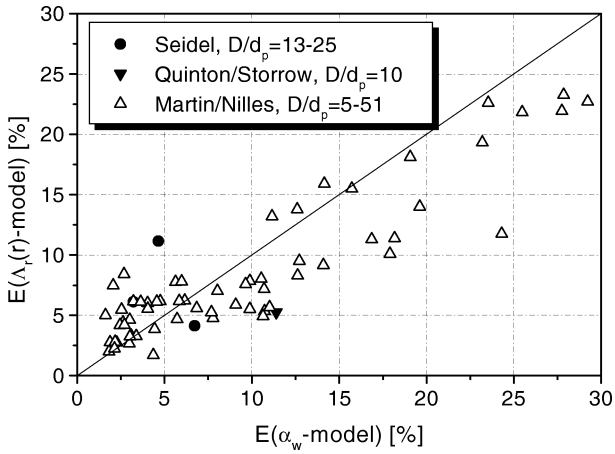


**Figure 12.** Comparison between the $\Lambda_r(r)$-model after Winterberg et al. [11] and the $\alpha_\mathrm{w}$-model of Martin and Nilles [19] with respect to the predictive performance for experiments in packed circular tubes with constant heat flux at the wall (data subgroup D3.2).

in the immediate vicinity of the wall. The temperature jump predicted by the $\alpha_\mathrm{w}$-model increases with increasing Reynolds number. In the total, the average error of the $\Lambda_r(r)$-model in respect to subgroup D3.2 is with $\overline{E}(\Lambda_r(r)) = 8.24\,\%$ even smaller than that of the $\alpha_\mathrm{w}$-model with $\overline{E}(\alpha_\mathrm{w}) = 9.38\,\%$ (*table I*). As the plot of *figure 12* shows, the advantage of the wall heat conduction model originates from the region of relatively large error indices, roughly corresponding to the region of relatively low Reynolds numbers. That experimental scatter is inherently contained in the definition of the error index of equation (2), and $E$ will not vanish completely for any model, can be clearly seen by the data of *figures 10* and *11*. Notice that pairs of points at $r/R = \mathrm{const}$ result from the measurement of temperatures at antidiametric positions of the bed by Martin and Nilles [19].

## 6. DISCUSSION

In the previous sections, the $\Lambda_r(r)$-model developed by Winterberg et al. [11] has been applied to experiments taken from literature which differ from the data the model has been fitted on in bed geometry and/or in the experimental boundary condition. In all cases, the prediction of the experimental data is satisfactory, in many cases even excellent. This means that the model may be used for all kinds of packed beds (packed circular tubes, rectangular channels and annular columns) and for all thermal boundary conditions. Its parameters remain invariant. In the total, the data base of the present

work is very comprehensive: 227 experiments with 2 045 measured temperatures covering Reynolds numbers, $Re_0$, from 1.5 to 1 818, average particles diameters, $d_p$, from 0.6 mm to 20 mm, and quotients between lateral bed dimension and particle diameter from 4.7 to 101.3 have been reevaluated.

Systematic comparison with the $\alpha_w$-model reveals that the $\Lambda_r(r)$-model can describe the data almost equally well for one and more accurately for six of seven data subgroups considered in the present work (*table I*). Since the overall predictive performance of the $\alpha_w$-model has also been found to be good, this is improvement from an already high level. To refrain from it may have been reasonable some years before, due to the relatively difficult numerical resolution of the $\Lambda_r(r)$-model; with today's hard- and software it is not. Furthermore, apart from the improved predictive accuracy, three additional arguments speak for the wall heat conduction concept:

- The $\Lambda_r(r)$-model has the conceptual advantage of putting complexity where it belongs (into the fundamental model equations), and keeping model parameters simple and coherent (see [11] as well as Section 1).
- In spite of overall similarity between the predictions of the two models, considerable temperature differences may occur locally, i.e. at the wall. Nonlinear phenomena in the bed can amplify this difference and magnify its impact, not only locally, but also in the total. Strong indication that this can be the case in packed beds with exothermic chemical reaction has been provided by Vortmeyer and Haidegger [10] and, more recently, by Hein [30].
- In contrast to the $\alpha_w$-model, the potential of the $\Lambda_r(r)$-approach has not been exhausted in the present application. One possible extension is to account for the interrelation between temperature and flow field which results from the dependence of fluid density and viscosity on temperature. An example (thermal channeling in packed bed reactors) is given, again, by Hein [30]. Membrane reactors, the combination of forced and free convection, and adsorber design could be further fields of interest. While remarks on the possible impact of flow maldistribution on the breakthrough behaviour of adsorbers exist in literature (e.g., [31, 32]) more thorough theoretical and experimental investigation is necessary.

The restriction of the present paper to nearly spherical particles will be relaxed in a separate communication. More experimental data with liquids are necessary, especially in the context of biotechnological applications.

## 7. CONCLUSION

Starting point of the present work has been a wall heat conduction model ($\Lambda_r(r)$-model) published recently by Winterberg et al. [11]. In this quasihomogeneous modelling approach for transport phenomena in packed beds, porosity, flow velocity and effective thermal conductivity are considered to be functions of the lateral space coordinate, i.e. of the distance from the wall. The model has been confronted with a comprehensive collection of experimental heat transfer data from literature, covering a range of Reynolds numbers, $Re_0$, between 1.5 and 1 818, of mean particle diameters, $d_p$, between 0.6 mm to 20 mm and of quotients between lateral bed dimension and particle diameter between 4.7 and 101.3. Experiments with different bed geometries (slab, annular channel, circular tube) and with different thermal boundary conditions at the wall or walls (constant temperature, constant heat flux, adiabatic) have been reevaluated. Very satisfactory agreement between model predictions and experimental results underlines the invariability of model parameters upon bed geometry and thermal boundary condition and the applicability of the $\Lambda_r(r)$-approach to a broad variety of practical situations. Remaining restrictions concern the particle shape (spherical) and the type of the fluid (only few data available for liquids).

Furthermore, systematic comparison between the $\Lambda_r(r)$- and the $\alpha_w$-model after Martin and Nilles [19] has been carried out on the basis of the experimental data. In the $\alpha_w$-model a temperature jump is postulated at the wall, while evenly distributed porosity, flow and conductivity are assumed. The comparison reveals good overall accuracy of the $\alpha_w$-model, but still better predictive performance of the $\Lambda_r(r)$-model. This, conceptual aspects, as well as better possibilities for considering temperature-dependent properties and simulating complex processes like reaction and adsorption justify the recommendation of the $\Lambda_r(r)$-model for practical use.

### *Acknowledgements*

The authors gratefully acknowledge the financial support of the present work by the Deutsche Forschungsgemeinschaft (DFG). The authors also express their thanks to Prof. H. Martin, University of Karlsruhe, Germany, Dr. M. Nilles, BASF, Germany, Dr. G. Sordon, Institute of Advanced Materials, Petten, Netherlands, as well as Dr. J. Gabor, Argonne National Laboratory, USA, for kindly providing original data.

## REFERENCES


[1] Westerterp K.R., van Swaaij W.P.M., Beenackers A.A.C.M., Chemical Reactor Design and Operation, Wiley, New York, 1984.

[2] Baerns M., Hofmann H., Renken A., Chemische Reaktionstechnik, Georg Thieme Verlag, Stuttgart, 1987.

[3] Tsotsas E., Wärmeleitung und Dispersion in durchströmten Schüttungen, in: VDI Wärmeatlas, Verein Deutscher Ingenieure, Düsseldorf, 1997, Chapter Mh.

[4] Roblee L.H.S., Baird R.M., Tierney J.W., Radial porosity variations in packed beds, AIChE J. 4 (1958) 460–464.

[5] Schwartz C.E., Smith J.M., Flow distribution in packed beds, Indust. Eng. Chem. 45 (1953) 1209–1218.

[6] Fahien R.W., Smith J.M., Mass transfer in packed beds, AIChE J. 1 (1955) 28–37.

[7] Cheng P., Vortmeyer D., Transverse thermal dispersion and wall channelling in a packed bed with forced convective flow, Chem. Eng. Sci. 43 (1988) 2523–2532.

[8] Kuo S.M., Tien C.L., Transverse dispersion in packed-sphere beds, in: Proc. Nat. Heat Transfer Conf., Vol. 1, 1989, pp. 629–634.

[9] Kalthoff O., Vortmeyer D., Ignition/extinction phenomena in a wall cooled fixed bed reactor, Chem. Engrg. Sci. 35 (1980) 1637–1643.

[10] Vortmeyer D., Haidegger E., Discrimination of three approaches to evaluate heat fluxes for wall-cooled fixed bed chemical reactors, Chem. Engrg. Sci. 46 (1991) 2651–2660.

[11] Winterberg M., Tsotsas E., Krischke A., Vortmeyer D., A simple and coherent set of coefficients for modelling of heat and mass transport with and without chemical reaction in tubes filled with spheres, Chem. Engrg. Sci. 55 (2000) 967–980.

[12] Tsotsas E., Über die Wärme- und Stoffübertragung in durchströmten Festbetten—Experimente, Modelle, Theorien, Vol. 223, VDI Fortschr. Ber., Reihe 3, VDI Verlag, Düsseldorf, 1991.

[13] Tsotsas E., Schlünder E.U., Heat transfer in packed beds with fluid flow: remarks on the meaning and the calculation of a heat transfer coefficient at the wall, Chem. Engrg. Sci. 45 (1990) 819–873.

[14] Winterberg M., Krischke A., Tsotsas E., Vortmeyer D., On the invariability of transport parameters in packed beds upon catalytic reaction, in: Proc. 2nd European Congress of Chemical Engineering, Montpellier, France, Récents Progrès en Génie des Procédés, Vol. 13, No. 65 (1999) pp. 205–212.

[15] Giese M., Strömung in porösen Medien unter Berücksichtigung effektiver Viskositäten, Dissertation, TU München, 1998.

[16] Giese M., Rottschäfer K., Vortmeyer D., Measured and modelled superficial flow profiles in packed beds with liquid flow, AIChE J. 44 (1998) 484–490.

[17] Zehner P., Schlünder E.U., Wärmeleitfähigkeit von Schüttungen bei mäßigen Temperaturen, Chem. Ing. Tech. 42 (1970) 933–941.

[18] Tsotsas E., Schlünder E.U., Some remarks on channelling and on radial dispersion in packed beds, Chem. Engrg. Sci. 43 (1988) 1200–1203.

[19] Martin H., Nilles M., Radiale Wärmeleitung in durchströmten Schüttungsrohren, Chem. Ing. Tech. 65 (1993) 1468–1477.

[20] Bauer R., Schlünder E.U., Effective radial thermal conductivity of packings in gas flow. Part I. Convective transport coefficient, Int. Chem. Engrg. 18 (1978) 181–188.

[21] Schröder K.J., Renz U., Elgeti K., Untersuchungen zum Wärmetransport in füssigkeitsdurchströmten Schüttungen, Forschungsbericht des Landes Nordrhein-Westfalen, No. 3037, 1981.

[22] Bey O., Eigenberger G., Bestimmung von Strömungsverteilung und Wärmetransportparametern in schüttungsgefüllten Rohren, Chem. Ing. Tech. 68 (1996) 1294–1299.

[23] Yagi S., Kunii D., Studies on heat transfer near wall surface in packed beds, AIChE J. 6 (1960) 97–104.

[24] Baddour R.F., Yoon C.Y., Local radial effective conductivity and the wall effect in packed beds, Chem. Engrg. Progr. Symp. Ser. Buffalo 57 (1961) 35–50.

[25] Gabor J.D., Heat transfer to particle beds with gas flows less or equal to that required for incipient fluidization, Chem. Engrg. Sci. 25 (1970) 979–984.

[26] Botterill J.S.M., Denloye A.O.O., A theoretical model of heat transfer to a packed or quiescent fluidized bed, Chem. Engrg. Sci. 33 (1978) 509–515.

[27] Sordon G., Über den Wärmetransport in Kugelschüttungen, Dissertation, Kernforschungszentrum Karlsruhe, 1988.

[28] Quinton J.H., Storrow J.A., Heat transfer to air flowing through packed tubes, Chem. Engrg. Sci. 5 (1956) 245–257.

[29] Seidel H.P., Wärmetransport, Stofftransport und Druckverlust in Füllkörperkolonnen, Dissertation, TU Dresden, 1965.

[30] Hein S., Modellierung wandgekühlter katalytischer Festbettreaktoren mit Ein- und Zweiphasenmodellen, Dissertation, TU München, 1998.

[31] Bey O., Strömungsverteilung und Wärmetransport in Schüttungen, Vol. 570, VDI Fortschr. Ber., Reihe 3, VDI Verlag, Düsseldorf, 1998.

[32] Otten W., Simulationsverfahren für die nichtisotherme Ad- und Desorption im Festbett auf der Basis der Stoffdaten des Einzelkorns am Beispiel der Lösungsmittel-adsorption, Vol. 186, VDI Fortschr. Ber., Reihe 3, VDI Verlag, Düsseldorf, 1989.


## APPENDIX

## Equations and parameters of the $\Lambda_r(r)$-model after Winterberg et al. [11]

### 1. Circular tube

Energy balance:

$$\frac{1}{r}\frac{\partial}{\partial r}\left[\Lambda_r(r) r \frac{\partial T}{\partial r}\right] = u_0(r)\rho_f c_f \frac{\partial T}{\partial z} - \Lambda_{ax}(r)\frac{\partial^2 T}{\partial z^2} \tag{A.1}$$

Porosity profile:

$$\psi(r) = \psi_\infty\left(1 + 1.36\exp\left[-5.0\,\frac{R-r}{d_\mathrm{p}}\right]\right) \qquad \text{(A.2)}$$

Velocity profile (extended Brinkman equation):

$$\frac{\partial p}{\partial z} = -f_1 u_0(r) - f_2\left[u_0(r)\right]^2 + \frac{\eta_\mathrm{eff}}{r}\,\frac{\partial}{\partial r}\left(r\,\frac{\partial u_0}{\partial r}\right) \qquad \text{(A.3)}$$

with the effective viscosity

$$\frac{\eta_\mathrm{eff}}{\eta_\mathrm{f}} = 2.0\exp\left(2.0\cdot 10^{-3} Re_0\right) \qquad \text{(A.4)}$$

the D'Arcy and Forchheimer factors

$$f_1 = 150\frac{(1-\psi(r))^2}{[\psi(r)]^3}\,\frac{\eta_\mathrm{f}}{d_\mathrm{p}^2} \quad \text{and} \qquad f_2 = 1.75\frac{(1-\psi(r))}{[\psi(r)]^3}\,\frac{\rho_\mathrm{f}}{d_\mathrm{p}} \qquad \text{(A.5)}$$

and the boundary conditions

$$r = 0 \longrightarrow \frac{\partial u_0}{\partial r} = 0$$
$$r = R \longrightarrow u_0 = 0$$

Effective axial thermal conductivity:

$$\Lambda_\mathrm{ax}(r) = \lambda_\mathrm{bed}(r) + \frac{Pe_0}{2}\lambda_\mathrm{f} \qquad \text{(A.6)}$$

with the molecular Péclet number for heat transfer

$$Pe_0 = \frac{\bar{u}_0 d_\mathrm{p}\rho_\mathrm{f} c_\mathrm{f}}{\lambda_\mathrm{f}} \qquad \text{(A.7)}$$

The effective thermal conductivity of the packed bed without fluid flow, $\lambda_\mathrm{bed}$, is calculated from a correlation provided by Zehner and Schlünder [17] as a function of the local porosity $\psi(r)$.

Effective radial thermal conductivity:

$$\Lambda_r(r) = \lambda_\mathrm{bed}(r) + K_1 Pe_0\,\frac{u_\mathrm{c}}{\bar{u}_0}\,f(R-r)\lambda_\mathrm{f} \qquad \text{(A.8)}$$

with

$$f(R-r) = \begin{cases} \left(\dfrac{R-r}{K_2 d_\mathrm{p}}\right)^2 & \text{for } 0 \le R-r \le K_2 d_\mathrm{p} \\ 1 & \text{for } K_2 d_\mathrm{p} < R-r \le R \end{cases} \qquad \text{(A.9)}$$

and

$$K_1 = \frac{1}{8} \qquad \text{(A.10)}$$

$$K_2 = 0.44 + 4\exp\left(-\frac{Pe_0}{50}\right) \qquad \text{(A.11)}$$

## 2. Annular channel

Energy balance: equation (A.1).

Porosity profile:

$$\psi(r) = \begin{cases} \psi_\infty\left(1 + 1.36\exp\left[-5.0\dfrac{r-r_\mathrm{cyl}}{d_\mathrm{p}}\right]\right) \\ \quad \text{for } r_\mathrm{cyl} \le r \le \dfrac{R+r_\mathrm{cyl}}{2} \\ \psi_\infty\left(1 + 1.36\exp\left[-5.0\dfrac{R-r}{d_\mathrm{p}}\right]\right) \\ \quad \text{for } \dfrac{R+r_\mathrm{cyl}}{2} < r \le R \end{cases} \qquad \text{(A.12)}$$

Velocity profile: equations (A.3)–(A.4) with the boundary conditions

$$r = r_\mathrm{cyl} \longrightarrow u_0 = 0$$
$$r = R \longrightarrow u_0 = 0$$

Effective axial thermal conductivity: equation (A.6).

Effective radial thermal conductivity: equation (A.8) with

$$f(R-r) = \begin{cases} \left(\dfrac{R-r}{K_2 d_\mathrm{p}}\right)^2 & \text{for } 0 \le R-r \le K_2 d_\mathrm{p} \\ 1 \quad \text{for } K_2 d_\mathrm{p} < R-r \le R - r_\mathrm{cyl} - K_2 d_\mathrm{p} \\ \left(\dfrac{r-r_\mathrm{cyl}}{K_2 d_\mathrm{p}}\right)^2 \\ \quad \text{for } R - r_\mathrm{cyl} - K_2 d_\mathrm{p} < R-r \le R - r_\mathrm{cyl} \end{cases} \qquad \text{(A.13)}$$

and $K_1$ and $K_2$ after equations (A.10) and (A.11).

## 3. Slab

Energy balance:

$$\frac{\partial}{\partial x}\left[\Lambda_x(x)\frac{\partial T}{\partial x}\right] = u_0(x)\rho_\mathrm{f} c_\mathrm{f}\,\frac{\partial T}{\partial z} - \Lambda_\mathrm{ax}(x)\,\frac{\partial^2 T}{\partial z^2} \qquad \text{(A.14)}$$

Porosity profile:

$$\psi(r) = \begin{cases} \psi_\infty\left(1 + 1.36\exp\left[-5.0\dfrac{x}{d_\mathrm{p}}\right]\right) \\ \quad \text{for } 0 \le x \le \dfrac{B}{2} \\ \psi_\infty\left(1 + 1.36\exp\left[-5.0\dfrac{B-x}{d_\mathrm{p}}\right]\right) \\ \quad \text{for } \dfrac{B}{2} < x \le B \end{cases} \tag{A.15}$$

Velocity profile:

$$\frac{\partial p}{\partial z} = -f_1 u_0(x) - f_2\left[u_0(x)\right]^2 + \eta_\mathrm{eff}\frac{\partial^2 u_0}{\partial x^2} \tag{A.16}$$

with the effective viscosity after equation (A.4) and $f_1$, $f_2$ after equations (A.5). The boundary conditions are

$$x = 0 \longrightarrow u_0 = 0$$

$$x = B \longrightarrow u_0 = 0$$

Effective axial thermal conductivity: equation (A.6) with $x$ instead of $r$.

Effective lateral thermal conductivity:

$$\Lambda_x(x) = \lambda_\mathrm{bed}(x) + K_1 Pe_0 \frac{u_\mathrm{c}}{\bar{u}_0} f(x)\lambda_\mathrm{f} \tag{A.17}$$

with

$$f(x) = \begin{cases} \left(\dfrac{x}{K_2 d_\mathrm{p}}\right)^2 & \text{for } 0 \le x \le K_2 d_\mathrm{p} \\ 1 & \text{for } K_2 d_\mathrm{p} < x \le B - K_2 d_\mathrm{p} \\ \left(\dfrac{B-x}{K_2 d_\mathrm{p}}\right)^2 & \text{for } B - K_2 d_\mathrm{p} < x \le B \end{cases} \tag{A.18}$$

and $K_1$ and $K_2$ after equations (A.10) and (A.11).